

MUFF: A Low-cost Motorized Positioner Developed by Additive Manufacturing to Obtain Multi-focus Images

Gustavo Leis da Silva¹^a, Jorge Stolfi¹^b and Helena Cristina da Gama Leitão²^c

¹State University of Campinas (UNICAMP), Campinas, SP, Brazil

²Federal Fluminense University (UFF) Niteroi, RJ, Brazil

Keywords: Optical Microscopy, 3D Printing, Multi-focus Stereo, Photometric Stereo, Arduino.

Abstract: Multifocal microscopy is an established technique to combine several reflected-light microscopy images of an object, each with a limited depth of focus, into a single image that shows the whole object in focus. Photometric stereo is an independent technique to recover the third dimension of an opaque object, given several images taken from the same viewpoint with different illumination conditions. We describe a low-cost motorized positioning device for the automatic acquisition of multiple reflected-light low-power microscope images of an object for combined multifocal and photometric stereo capture of millimeter-scale objects. The device automatically varies the microscope-to-object distance and the light direction, under control of an Arduino microcontroller. The device consists of a supporting frame, a microscope holder with motorized vertical displacement, an illumination stage with multiple light sources, and control electronics. The mechanical and structural parts are largely 3D-printed. The electronics is based on the Arduino microcontroller. The device is driven through an USB cable by a Python program that runs on a PC.


1 INTRODUCTION


Multi-focus Stereo: An optical microscope usually can focus only on those points of the target object that lie in a narrow range of distances from the objective lens; that is, between two close planes perpendicular to the optical axis. The distance ϵ between these planes, called *depth of field*, is inversely proportional to the magnification and to the effective aperture of the microscope (Ciciliato and Chiquito, 1995). If the target object cannot fit between these two planes, it is necessary to acquire several images J_i for $i = 1, 2, \dots, n$, varying the object-lens distance, so that every visible point of the object is in focus in at least one of the images. The number n of images must be at least H/ϵ , where H is the total extent of the object in the Z -direction. These images then can be composited into a single *multi-focus image* (MFI) \tilde{J} that shows the whole object in focus. See Figure 1. As a by-product, this technique also provides information about the three-dimensional shape of the object, in the form of a *height map* — an image \tilde{Z} that,


for each pixel of the combined image, specifies the approximate Z coordinate of the point on the object's surface that is visible at that pixel. This method to recover the 3D shape of the object is known as *shape from focus* (Nayar, 1989; Fernandes and Torreão, 2010), *depth from focus* (Grossmann, 1987) or *multi-focus stereo* (MFS).

The principles of multi-focus stereo were described in 1987 by Grossmann (Grossmann, 1987) and in 1989 by Nayar (Nayar, 1989). A brief survey of the field was provided in 2012 by Thiery and Green (Thiery and Green, 2012), and also in 2003 by Zamofing et al. (Zamofing and Hugli, 2004). Applications of MFI and MFS include the imaging of minerals (Thiery and Green, 2012), manufacturing (Zamofing and Hugli, 2004), paleontology (Bercovici et al., 2009), and archaeology (Plisson and Zotkina, 2015).

Photometric Stereo: Another technique for capturing the three-dimensional shape of an object uses several images $J^{(k)}$ for $k = 1, 2, \dots, m$, taken from the same viewpoint but under different illuminations (Woodham, 1980; Coleman and Jain, 1982). Analysis of these images yields *surface normal map* \hat{N} and an *intrinsic color map* \hat{A} , that specify the incli-

^a  <https://orcid.org/0000-0002-3834-412X>

^b  <https://orcid.org/0000-0002-3159-4839>

^c  <https://orcid.org/0000-0002-4722-4963>

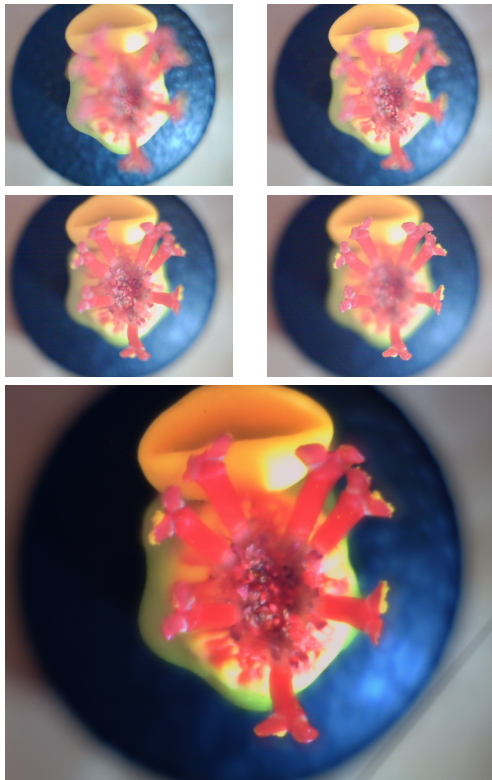


Figure 1: Illustration of the multi-focus imaging technique. The four images at top are frames J_1 , J_9 , J_{17} , and J_{25} of a 25-frame stack. The larger image at bottom is the sharp composite image \tilde{J} .

nation and per-channel albedo of the visible surface, respectively, at each pixel. The slope information then can be integrated to obtain a height map \hat{Z} (Saracchini et al., 2012). The number m of images must be at least 6 to provide sufficient data for this computation (Leitão et al., 2008), but several more are needed if there are complicating factors like projected shadows, glossy highlights, significant self-lighting, etc. See figure 2. This technique is called *Photometric stereo* (PMS).

The physical principles of photometric stereo have been known since the development of photometry in 1760 by Lambert (Lambert, 1760), and their use by astronomers in the early 20th century (Rindfleisch, 1966). The first mathematically sound formulation was given by Woodham in 1980 (Woodham, 1980). The method has since been improved and generalized, e. g. by Hertzmann (Goldman et al., 2010), Saracchini et al. (Saracchini et al., 2011), and Quéau et al. (Quéau et al., 2015). Photometric stereo can be used for scenes of arbitrary size, from planets (with the sun as light source) (Rindfleisch, 1966) to bacteria (by varying the position of the backscatter detector in a scanning electron microscope) (Miyamoto et al.,

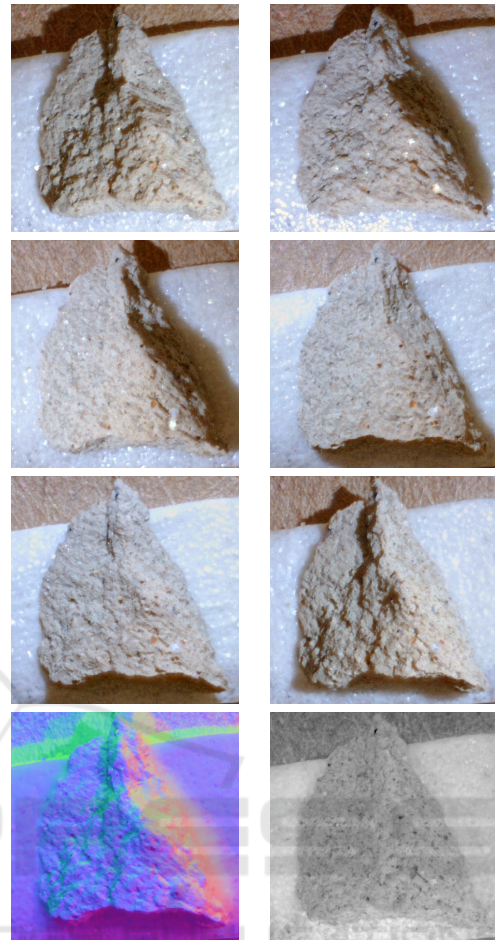


Figure 2: Example of the photometric stereo technique. The top six images are photos $J^{(1)}, \dots, J^{(6)}$ of a small rock/plaster fragment under different lighting conditions. The images at bottom are the color-coded surface normal map \hat{N} and the intrinsic color map \hat{A} computed from the above.

2017).

The two techniques are largely complementary, because MFS works best when the object's surface is discontinuous or has sharp details, whereas PMS works best when the surface is smooth and featureless. Therefore, combining the two techniques promises to yield better reconstructions than what each method can provide on its own. For this combined approach, one must obtain images $J_i^{(k)}$ for n microscope-to-object distances $i = 1, 2, \dots, n$ and m illumination sources $k = 1, 2, \dots, m$. The multifocal stereo technique is used to obtain a combined sharp image $\tilde{J}^{(k)}$ for each light source k , and a tentative height map $\tilde{Z}^{(k)}$. Then the photometric stereo technique is applied to these images, to obtain a single final height map \hat{Z} and the intrinsic color map \hat{A} .

2 THE POSITIONER

One obstacle to this combined multi-focus/photometric stereo idea is the large number (mn) of images that must be obtained, which may reach a hundred or more. In order to alleviate this problem, we built a simple motorized positioning device that captures all those images automatically, varying the distance between the microscope and the object and the illumination of the same. See Figure 3.

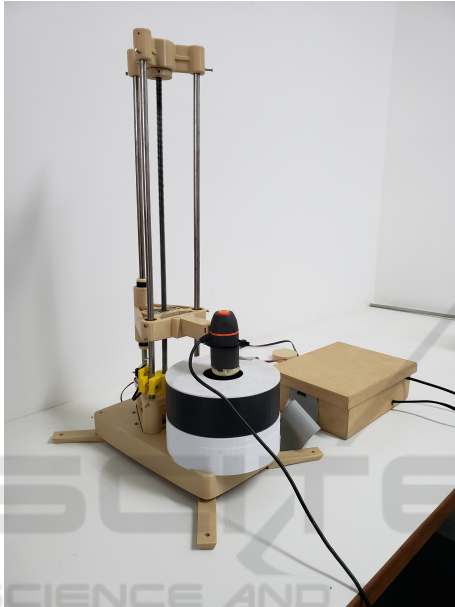


Figure 3: Image of the motorized positioner, with a Celestron Mini Handheld Digital Microscope installed.

The frame is built from 3D-printed plastic elements and other easily-obtained parts. The stepper motor (that varies the focus plane) and the LED light sources (that provide the variable illumination) are controlled by an Arduino processor and by software running on a PC. This original design may be a viable alternative to commercial motorized microscope stands (Silva, 2020).

As seen in Figure 3, the positioner consists of a stationary supporting *frame*, a moving *carriage* that holds the microscope, and a *light box* that surrounds the target object and holds the light sources. The carriage is displaced vertically along three fixed guide rails by a screw, driven by a stepper motor in the base of the frame. A separate box contains the dedicated electronics that control the stepper motor and the light sources. The electronics and the camera are connected to the PC by two separate USB cables.

2.1 Operation

Once the positioner is powered up and the operating software is running, all further user interaction takes place through a program running on the hosting PC, that continually displays the image seen by the camera, in real-time.

Specifically, for each job the user commands the positioner to raise the camera out of the way, places the target object on the stage inside the light-box, and commands the positioner to lower the camera until its focus plane is completely below the visible parts of the target. That action defines the first focus plane position $\bar{z}_1 = 0$. The user then specifies the number n of focus positions, the vertical spacing δ between them, and the number m of illumination conditions. The program then automatically captures the nm images $J_i^{(k)}$, looping on k for each camera position i . Each captured image is displayed by the program, on a separate window, and saved as a disk file on the PC's disk.

3 STRUCTURAL AND MECHANICAL PARTS

Most structural parts of the frame and carriage are made of polylactic acid (PLA) thermoplastic, and were manufactured with a desktop 3D printer (MAKERBOT REPLICATOR 2). The geometric models were created by us, using the CAD software supplied with the printer.

Other major structural and mechanical components of the system include three vertical steel rails, a threaded rod and its sliding nut, two clamping springs, a stepper motor, and six roller bearings (two rotary and four linear). These parts are held together mostly by set screws that are self-threaded into the plastic parts.

3.1 Static Frame

The static frame of the positioner consists of a base with four extended feet, a lower rail support, an upper rail support, a limit switch holder, and three vertical steel columns. See Figure 4. The columns are smooth solid steel bars, 8 mm in diameter, that double as structural elements and as rails for the carriage.

The lower rail support is a single 3d-printed piece consisting mainly of three thick-walled tubular rail holders, with 8 mm internal diameter, connected by straps in an equilateral triangular prism; and a cubical motor enclosure, open at the bottom, nestled between

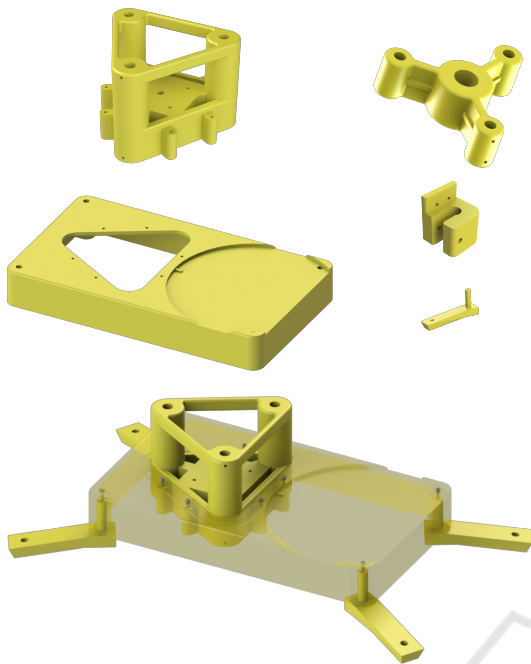


Figure 4: The plastic parts of the frame. Top row: the lower and upper rail supports. Middle row: the base, limit switch holder, and one of the four feet. Bottom: how the lower rail support and the feet are attached to the base.

those tubes. Each rail fits snugly in the vertical hole of its holder, and is secured by two set screws. The position and radial orientation of the set screws helps to ensure that the guides are parallel and equidistant, in spite of play in the vertical hole and deformation of the plastic.

The upper rail support too is a single 3D-printed piece. Its purpose is to hold upper ends of the three rail guides and of the driving screw in the proper relative positions. It consists of three thick-walled tubular guide holders, arranged in an equilateral triangle; and a central bearing holder. These four sections are held together by three radial arms. As in the lower support, each rail is secured to the upper support by two self-threading set screws.

The base is a hollow rectangular box, measuring $240\text{mm} \times 140\text{mm} \times 33\text{mm}$ and 3 mm thick, fully open at the bottom. On the top side it has a triangular opening where the lower support fits, and a circular depression to hold the light box (see below). Attached at each corner, on the inside, there is a short vertical tube that can hold a plastic foot, secured by a screw from the top of the box. The lower rail support is attached to the base by six screws.

The limit switch holder is a plastic part that is clamped around one of the guide rails, near the bottom. It holds a microswitch that is positioned and

wired in such a way that the motor turns off immediately when the carriage reaches the lower end of its range. This detail is meant to protect the motor from overheating and to prevent the camera from hitting the target object inside the light box. The vertical position of the holder can be adjusted according to the camera dimensions.

3.2 The Carriage

During use, the camera is firmly attached to a plastic carriage that slides on the three rails, driven by a threaded rod connected to the stepper motor in the base. It has three separately printed plastic parts: a chassis, a nut counter-plate, and an interchangeable camera holder. See Figure 5.

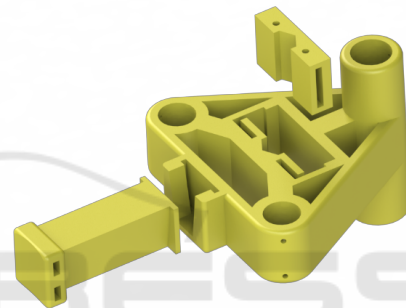


Figure 5: The three plastic parts of the carriage. The bushings, springs, and split nut are not shown.

The chassis, somewhat similar to the lower support, consists of three vertical tubes connected by straps in an equilateral triangle. However, the vertical hole in each tube is wider, and the tube in the back is more than twice as long as the other two. Two stainless steel linear motion bearings (type LM08UU, $15\text{mm} \times 24\text{mm}$, with 8 mm internal diameter) are inserted in the two tubes at the front and secured by two set screws each. Two teflon bushings with the same dimensions are inserted at opposite ends of the rear tube and each is held by a set screw. All six set screws are oriented radially. This configuration of bearings and bushings provides four non-coplanar points of contact with the rails, that prevent the chassis from tilting in any direction; but still allows the chassis to slide up and down with low static and dynamic friction.

At the center of the chassis there is an opening with a vertical channel that is meant to hold an M8 hexagonal nut, about 28 mm long, split lengthwise through two opposite faces. In the assembled carriage, the halves of the nut are pressed against the drive screw by a plastic plate with a matching vertical channel, and two steel springs (two 25 mm binder

clips without the handles). One leaf of each spring is fixed to the pressure plate by a self-threaded screw, while the other leaf slides down into a slot in the chassis. The pressure from these springs removes any play that might have existed between the nut and the chassis, thus ensuring that the vertical position of the latter accurately tracks the rotation of the screw.

The front of the chassis has a pair of slots where the camera holder can be inserted. The main purpose of the latter is to position the camera so that its optical axis matches the axis of the light box. This two-part design rigidly fixes the camera to the chassis, but still allows it to be quickly removed for other uses, or swapped by a different camera, without disassembling the positioner. Also, a camera with different diameter or shape can be accommodated by fabricating just a new holder (rather than a new chassis).

For the hand-held digital microscope that we used in our tests, we fabricated a holder (shown in Figure 5) with an arm about 100mm long ending with a concave plate. The camera was secured against that plate by two nylon zip-ties, inserted through a pair of horizontal holes.

3.3 The Driving Mechanism

The mechanism that drives the carriage consists of a stepper motor, mounted inside the lower support, and a drive screw that for the full height of the frame, with plastic connectors at each end. The motor is a NEMA 17 model with 1.1 Nm of torque and 200 steps per turn. The drive screw is a coarse-threaded M8 (8 mm diameter, 1.25 mm pitch) steel rod bought at a hardware store.

Torque Coupler: Experiments with previous iterations of the device led us to suspect that, because of the frame's rigidity, slight misalignments between the motor axis and the axis of the carriage's nut were generating excessive lateral forces greatly increased friction in the latter, causing slippage in the stepper motor.

To avoid this potential problem, we designed a plastic torque coupler to connect the motor to the drive screw. See Figure 6 (left). It consists of two "flanges" attached to the motor's shaft (A) and to the lower end of the screw (B) by set screws. These two parts are connected through a transfer disk (C), with two small teeth on each face. Each pair of teeth slides along a slots cut into the flat face of the adjacent flange. The teeth pairs on the two sides are 90 degrees offset to each other. Two thin disks of a hard and smooth PET-like plastic, with slots cut out for the

teeth, are inserted between the three disks to reduce friction.

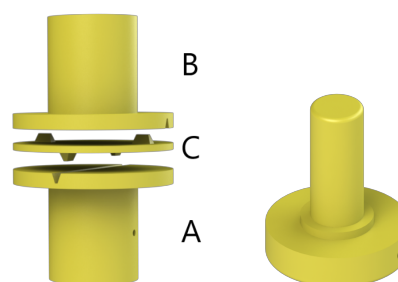


Figure 6: Left: the torque/angle coupler between motor and drive screw. Right: the adapter for the top of the drive screw.

The teeth and slots tightly couple the rotation angle of the screw to that of the motor shaft, and transmit the full torque of the latter to the former. However, any misalignment of the two will be accommodated by lateral shifts of the middle disk, even as the screw turns, with little lateral stress being felt by either of them.

Upper Bearing Adapter: The upper end of the drive screw is inserted in a plastic adapter (Figure 6, right), that fits into a standard roller bearing that in turn fits into a cavity on the bottom side of the upper support.

3.4 The Light-box

The purpose of the light-box is to provide a controlled and repeatable illumination for the target object, that is automatically varied as required by the PMS method. See Figure 7. It consists of a low cylindrical platform (E), a specimen stage (D), a light diffuser dome (C), an illumination section (B), and a lid (A).

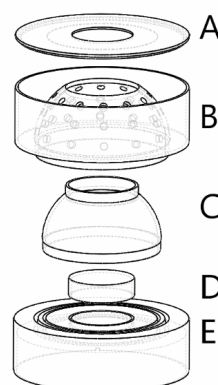


Figure 7: Exploded diagram of the light box.

These parts, printed in white PLA, are not fastened together, so that the stage can be easily accessed, and any part of the light box can be excluded, replaced, or modified if necessary. The platform E is open at the bottom and fits into a circular depression on top of the base; its purpose is to ensure that, when the carriage is at its lowest position, the focus plane of the camera lies below the target object. The stage D raises the target object a bit further so as to improve its illumination. The diffusing dome C, thin and translucent, may be used to obtain more uniform and smoother lighting of the target, if so desired.

The illumination section B is a single plastic part consisting of a dome that holds the LED light sources and a cylindrical enclosure that, together with the lid A, protects their terminals and wiring. The lid has an opening just wide enough for the camera. The internal surfaces facing the target are painted matte black.

The device currently has 24 LEDs, arranged in two rings of 12. A third ring of holes on the dome could hold another 12 light sources. Each LED has an independent connection to the electronics box through a flat 40-wire data cable that exits through a slot in the back of the section. For greater flexibility, each LED is held by an individual 3D printed sleeve (not shown) that is plugged into the corresponding hole of the light dome. This arrangement can accommodate LEDs of various sizes, holds them more firmly, and allows their orientation to be individually adjusted.

4 ELECTRONICS

The main component of the dedicated electronics are two 10cm × 10cm printed circuit boards (PCBs) of the stripboard type, a power supply, and a motor power drive unit. The electronics circuitry spans also the 24 LEDs in the light box, the overrun sensing microswitch, and the windings of the stepper motor. See Figure 8. These components are housed in a low 20cm by 25cm MDF box, seen in Figure 3.

The central component of the electronics is an Arduino Nano V3 microcontroller (AG, 2017) mounted on one of the PCBs. All components, except the motor driver, are powered by the +5V line from the USB cable, through the Arduino. The rest of the electronics can be conceptually divided into two subsystems: motion control and lighting control.

4.1 Motion Control

The motion control subsystem applies current pulses with the proper polarity and timing to the motor wind-

ings. A standard power drive unit (Texas Instruments DRV8825), fed by a switching power supply type MS-50-12 (10A, 12V, 60W) is used to convert the binary 0/5V output signals of the Arduino to the $\pm 12V$ voltage and high currents required by the motor, and also to provide over-current and temperature overload protection. The Arduino output ports D2, D3, and D4 are connected to the drive's Enable, Step, and Direction input pins of the power drive. Outputs 1A, 1B, 2A, and 2B of the drive are connected to the motor winding terminals.

The motion control circuitry includes the carriage travel limit sensor, a type MSW-14B micro switch connected to the Arduino +5V and D10 ports. When the switch is activated, the Arduino firmware will prevent the motor from turning any further in the direction that lowers the carriage. This safety feature could also be used by the controlling script to place the carriage at a specified absolute position, independently of its current state.

4.2 Lighting Control

The light sources currently in use are 24 LEDs, each producing 10000mcd of white light with color temperature 5500–6000K. They are driven by a chain of three serial-to-parallel demultiplexers (Texas Instruments 74HC595), each with 8 binary 0/+5V outputs. A 270 Ω resistor limits the current through each LED to the nominal maximum of 18.5 μ A. The state of the LEDs can be changed by the Arduino by sending 24 bits serially through port D6.

5 SOFTWARE

The device's software consists of a firmware stored and executed by the Arduino, and a script that runs on a PC.

5.1 Arduino Firmware

The embedded program `muff_firmware` was written in the standard Arduino C-like programming language. It uses various free libraries, including the `AccelStepper` module for stepper motor control (McCauley, 2017). It receives encoded commands and parameters through the Arduino's serial communication (USB) port. Each command consists of one byte of operation code, and (depending on the operation) up to four bytes of operand. The available commands include starting the motor in cruise (constant speed) mode, up or down, stopping the motor, raising or lowering the carriage by a specified

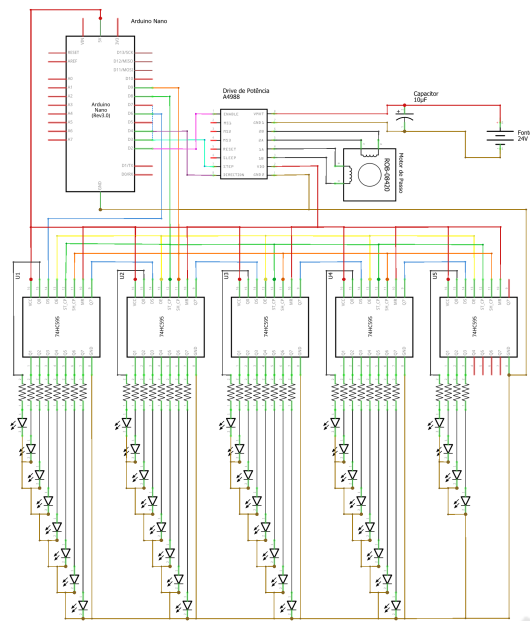


Figure 8: Circuit diagram of the dedicated electronics. Currently only 24 of the 36 LEDs are installed, thus only the first three multiplexers are needed.

distance, and turning a specific LED on or off. The complete list is provided in the software’s documentation (Silva et al., 2019).

5.2 Image Acquisition Script

The image acquisition script `muff_capture` is written in the Python language (Silva et al., 2019). It performs two main functions: (a) send to the Arduino the commands needed to position the camera and turn on the proper LEDs for each image $J_i^{(k)}$ to be acquired; and (b) capture the image from the camera, saving it to disk. Currently the script relies on the open-source software `uvcapture` for the latter task. These actions are fully automatic, as described in section 2.1. The script also lets the user issue individual firmware commands, e. g. for testing or debugging.

6 CONCLUSIONS

We described a simple device to facilitate capture of the large number of images required to combine the techniques of multi-focus and photometric stereo for millimeters-scale objects, by automatically varying the position of the microscope camera and the sample illumination conditions. The device requires access to a 3D printer and a few cheap and easily obtainable parts. The device can position the camera with sub-

millimeter precision and provide up to 24 independent lighting conditions. These parameters are usually sufficient for good MFS/PMS analysis.

Many possible improvements to the positioner suggest themselves, such as a more precise driving mechanism and an angular encoder to remove the risk of slippage. Indeed, a copy of this device incorporating these improvements was recently built by Alysson Mazoni for use at the Geosciences Department of UNICAMP.

Another very desirable improvement would be a mechanism to move the specimen stage horizontally, so that centimeter-scale objects can be automatically digitized with overlapping MFS/PMS stacks. Also, a mechanism to tilt the stage, even if only by 10-30 degrees, would make it possible to combine MFS and PMS with *geometric stereo* (GMS), that infers the third dimension from multiple images taken from different directions.

ACKNOWLEDGMENTS

This project was partly funded by CNPq (grant 301016/92-5), FAPERJ, UFF (grant PIBINOVA/PDI-2018), and FAPESP (grant 2013/07699-0).

REFERENCES

AG, A. (2017). Getting started with the ARDUINO NANO. At <https://www.arduino.cc/en/Guide/ArduinoNano>.

Bercovici, A., Hadley, A., and Villanueva-Amadoz, U. (2009). Improving depth of field resolution for palynological photomicrography. *Palaeontologia Electronica*, 12(2):12.

Ciciliato, V. and Chiquito, J. G. (1995). Modelamento do microscópio óptico como um sistema linear variante com o deslocamento. In *Anais do 13^o Simp. Bras. de Telecomunicações (SBrT 1995)*, volume 1, pages 258–263.

Coleman, E. and Jain, R. (1982). Obtaining 3-dimensional shape of textured and specular surface using four-source photometry. *Computer Graphics and Image Processing*, 18:308–328.

Fernandes, J. L. and Torreão, J. R. A. (2010). Shape from shading through photometric motion. *Pattern Anal. Appl.*, 13(1):35–58.

Goldman, D. B., Curless, B., Hertzmann, A., and Seitz, S. M. (2010). Shape and spatially-varying BRDFs from photometric stereo. *IEEE Transactions on Pattern Analysis and Machine Intelligence*, 32(6):1060–1071.

Grossmann, P. (1987). Depth from focus. *Pattern Recognition Letters*, 5(1):63–69.

- Lambert, J. H. (1760). *Photometria, sive de Mensura et Gradibus Luminis, Colorum et Umbrae*. E. Klett.
- Leitão, H. C. G., Saracchini, R. F. V., and Stolfi, J. (2008). Matching photometric observation vectors with shadows and variable albedo. In *Proc. the 21st Braz. Symp. on Computer Graphics and Image Processing (SIBGRAPI 2008)*, pages 179–186.
- McCauley, M. (2017). Accelstepper library for Arduino. At <http://www.airspayce.com/mikem/arduino/AccelStepper/>.
- Miyamoto, A., Matsuse, H., and Koutaki, G. (2017). Robust surface reconstruction by design-guided SEM photometric stereo. *Measurement Science and Technology*, 28(4).
- Nayar, S. K. (1989). Shape from focus. Technical Report CMU-RI-TR-89-27, Robotics Institute, Carnegie Mellon Univ.
- Plisson, H. and Zotkina, L. V. (2015). From 2D to 3D at macro- and microscopic scale in rock art studies. *Digital Applications in Archaeology and Cultural Heritage*, 2(2–3):102–119.
- Quéau, Y., Lauze, F., and Durou, J.-D. (2015). A L^1 -TV algorithm for robust perspective photometric stereo with spatially-varying lightings. In *Intl. Conf. on Scale Space and Variational Methods in Computer Vision*, pages 498–510.
- Rindfleisch, T. (1966). Photometric method for Lunar topography. *Photometric Engineering*, 32(3):262–276.
- Saracchini, R. F. V., Stolfi, J., and Leitão, H. C. G. (2011). A uniform grid structure to speed up example-based photometric stereo. *IEEE Trans. on Image Processing*, 20(12):3495–3507.
- Saracchini, R. F. V., Stolfi, J., Leitão, H. C. G., Atkinson, G. A., and Smith, M. L. (2012). A robust multi-scale integration method to obtain the depth from gradient maps. *Computer Vision and Image Understanding*, 116(8):882–895.
- Silva, G. L. (2020). Posicionador automatizado para aplicação das técnicas de multifocal stereo e photometric stereo para objetos microscópicos. Final undergraduate project, Federal Fluminense Univ., Electrical Eng. Dept. (in Portuguese).
- Silva, G. L., Stolfi, J., and Leitão, H. C. G. (2019). Muff positioner - software, diagrams, and stl files. At <http://www.ic.uff.br/~hcg1/Muff-index.html>.
- Thiery, V. and Green, D. I. (2012). The multifocus imaging technique in petrology. *Computers & Geosciences*, 45:131 – 138.
- Woodham, R. J. (1980). Photometric method for determining surface orientation from multiple images. *Optical Engineering*, 19(1):139–144.
- Zamofing, T. and Hugli, H. (2004). Applied multifocus 3D microscopy. In *Proc. SPIE*, volume 5265, pages 134–144.